

Engineering Quantum-Enhanced Transport by Supertransfer

Adesh Kushwaha and Ivan Kassal*

School of Chemistry, University of Sydney, NSW 2006, Australia

Collective behaviour of the components of a quantum system can significantly alter the rates of dynamical processes within the system. A paradigmatic collective effect is superradiance, the enhancement in the rate that radiation is emitted by a group of emitters relative to that emitted by independent emitters. Less studied are collective effects in energy transport, notably supertransfer, the enhancement of the rate of energy transfer from donors to acceptors due to delocalised excitations. Despite its proposed significance in photosynthesis, there has been no direct experimental detection of supertransfer because, in biological or molecular systems, delocalisation cannot be turned on and off to evaluate its effect on energy transfer. Here, we show that supertransfer could be directly observed using a quantum device based on a superconducting circuit. The programmability and control offered by an engineered device would allow controllable delocalisation of quantum states, giving full tunability over supertransfer. Our guidelines for engineering supertransfer could inform the design of future quantum-enhanced light harvesters.

Collective (or cooperative) effects occur when the rates of dynamical processes in a many-body system depend on its components' interactions with each other. The first collective effect to be studied was superradiance of a radiating gas, where the delocalisation of the system's wavefunction across many atoms increases the rate of emission [1, 2]. The collective effect that is the opposite of superradiance is superabsorption, where delocalisation over many particles enhances the absorption rate of radiation [3, 4], a feature that is exploited in proposed quantum batteries [4–6].

Collective effects also occur in transport, where supertransfer is the collective enhancement of transport rates due to delocalisation [7–12]. For example, collective transport enhancements are known in both non-radiative energy transfer and in electron transfer, where they are described by, respectively, generalised Förster resonant energy transfer (gFRET) [13] and generalised Marcus theory (gMT) [12]. The rate enhancements due to supertransfer can improve the efficiency of energy transport in quantum systems [14]. As a result, supertransfer is believed to contribute to the high efficiency of light harvesting in certain photosynthetic antenna complexes, especially those of purple bacteria [11, 13, 15–17]. The possible role of collective effects in photosynthesis has inspired suggestions for using them to improve the efficiency of artificial light-harvesting devices; in fact, of all possible coherent enhancements of light harvesting, supertransfer is the one most likely to be achievable in natural sunlight [14, 18, 19].

Despite its promise to enhance transfer efficiency, there have been no direct experimental demonstrations of supertransfer. In molecular or photosynthetic systems, this is likely due to the impossibility of turning coherent effects on and off, making it impossible to compare normal transfer and supertransfer in the same system to show a clear enhancement due to delocalisation.

Here, we propose an artificial quantum device that allows tuning the delocalisation in a way that could be used to definitively show supertransfer. Our proposal is based on superconducting circuits, which offer programmability and precise control for studying complex quantum phenomena [20–22]. Furthermore, we present design guidelines to optimise energy transfer using supertransfer, which could be incorporated into future quantum-enhanced light-harvesters.

I. SUPERTRANSFER

Supertransfer [7] is the enhancement of the transfer rate from an aggregate (or group) of donor sites to an aggregate of acceptor sites due to coherent delocalisation among strongly interacting donors, acceptors, or both. In the following, we will use the language of energy transfer, where the donors are initially excited and transfer excitation energy (or excitons) to the acceptors; however, our results hold true for other types of supertransfer, for example of charge. The transfer rate γ is defined by the rate of change of the acceptor population P_A ,

$$\frac{dP_A}{dt} = \gamma P_D, \quad (1)$$

where P_D is the population of the donor aggregate.

The rate γ can be derived through time-dependent perturbation theory or Fermi's golden rule [23] when the coupling between the donor and acceptor aggregates is weak compared to the system-environment coupling. We assume that donor and acceptor sites are coupled through $H_{DA} = \sum_{jk} V_{jk}^{DA} |A_k\rangle \langle D_j| + \text{h.c.}$, where the states $|D_j\rangle$ and $|A_k\rangle$ describe an excitation on an individual donor or acceptor site. The rate of transfer from donor eigenstate $|i\rangle$ to acceptor eigenstate $|f\rangle$ is then

$$\gamma = \frac{2\pi}{\hbar} |\langle i| H_{DA} |f\rangle|^2 \nu(\omega), \quad (2)$$

where $\nu(\omega)$ is the density of states near $|f\rangle$.

Normal transfer occurs when both eigenstates $|i\rangle$ and $|f\rangle$ are localised on individual sites, which means that each donor site independently transfers energy to acceptor sites. The transfer rate from localised state $|i\rangle = |D_j\rangle$ to localised state $|f\rangle = |A_k\rangle$ is

$$\gamma_{\text{loc}} \propto |\langle A_k| H_{DA} |D_j\rangle|^2. \quad (3)$$

The same result is obtained if the initial donor state is in the mixed state $\sum_j p_j |D_j\rangle \langle D_j|$, assuming that all the V_{jk}^{DA} are equal. In that case, the rate is

$$\gamma_{\text{mix}} \propto \sum_j p_j |\langle A_k| H_{DA} |D_j\rangle|^2 = \gamma_{\text{loc}}, \quad (4)$$

assuming $\nu(\omega)$ remains constant.

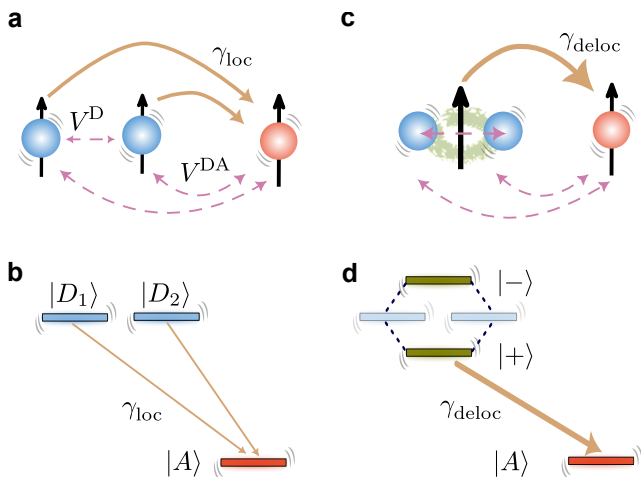


Figure 1. **Simplest example of supertransfer.** Two degenerate donor sites (blue) interact through a dipole-dipole interaction (purple) with each other and with an acceptor site (red). **a) Normal transfer.** An excitation transfers from weakly coupled donor sites to the acceptor. Because of their weak coupling, the donors are in a mixed state of $|D_1\rangle$ and $|D_2\rangle$, and transfer to $|A\rangle$ occurs at a rate of γ_{loc} . **b)** The energy diagram corresponding to (a). **c) Supertransfer.** The excitation transfers from strongly coupled donors in the delocalised eigenstate $|+\rangle = (|D_1\rangle + |D_2\rangle)/\sqrt{2}$, with a rate γ_{deloc} . The transition dipole of $|+\rangle$ is larger than the transition dipoles of local states, leading to faster transfer, $\gamma_{deloc} = 2\gamma_{loc}$. **d)** The energy diagram corresponding to (c).

By contrast, supertransfer occurs between delocalised eigenstates. To show the enhancement due to delocalisation, we consider an excited delocalised eigenstate of the donor aggregate,

$$|D_\alpha\rangle = \sum_{j=1}^{N_D} c_{\alpha j} |D_j\rangle, \quad (5)$$

where N_D is the number of donor sites. For example, in a fully delocalised donor state, $c_{\alpha j} = 1/\sqrt{N_D}$, while a localised state ($|D_{j'}\rangle$) has $c_{\alpha j} = \delta_{jj'}$. Similarly, we take a delocalised eigenstate of the acceptor aggregate,

$$|A_\beta\rangle = \sum_{k=1}^{N_A} c_{\beta k} |A_k\rangle. \quad (6)$$

The transfer rate between the delocalised eigenstates $|i\rangle = |D_\alpha\rangle$ and $|f\rangle = |A_\beta\rangle$ is

$$\gamma_{deloc} \propto |\langle A_\beta | H_{DA} | D_\alpha \rangle|^2 = \left| \sum_{j,k} c_{\alpha j} c_{\beta k}^* V_{jk}^{DA} \right|^2. \quad (7)$$

This rate is maximised for completely delocalised eigenstates ($c_{\alpha j} = 1/\sqrt{N_D}$ and $c_{\beta k} = 1/\sqrt{N_A}$),

$$\gamma_{deloc}^{\max} = \gamma_{loc} \left| \sum_j \sum_k \frac{1}{\sqrt{N_D}} \frac{1}{\sqrt{N_A}} \right|^2 = N_D N_A \gamma_{loc}, \quad (8)$$

meaning that delocalisation can enhance the transfer rate by a factor of $N_D N_A$ over the normal transfer rate.

In general, we will describe as supertransfer any increase in the transfer rate, i.e., any situation where

$$\gamma_{loc} \leq \gamma_{deloc} \leq N_D N_A \gamma_{loc}. \quad (9)$$

The smallest system with supertransfer requires $N_D = 2$ and $N_A = 1$ (fig. 1), resulting in $\gamma_{loc} \leq \gamma_{deloc} \leq 2\gamma_{loc}$. It is also possible to attain subtransfer, where the rate can be reduced below γ_{loc} , potentially to zero, by the destructive interference caused by coefficients $c_{\alpha j}$ and $c_{\beta k}$ of opposite sign.

The transfer rate can even increase further if the number of excitations exceeds the previously assumed value of one. In that case, the rate can scale with the size of the system as $O(N_D^2 N_A)$ [9]. However, we do not consider the multi-excitation case further.

The transfer rate allows us to define the transfer efficiency, a key figure of merit, especially in light harvesting. For efficient transfer, energy must be transferred to the acceptor aggregate before it is lost to recombination processes, which we assume to occur at some rate γ_{loss} . We define the efficiency as $\eta = \gamma/(\gamma + \gamma_{loss})$. Supertransfer increases η as it increases the transfer rate γ for a given γ_{loss} . Another mechanism to improve efficiency is to suppress loss rates [24, 25].

II. MODEL

To construct a demonstration of supertransfer, we consider aggregates of N_D donors and N_A acceptors, which are all coupled to each other and to an environment, with the Hamiltonian

$$H = H_D + H_A + H_{DA} + H_{DE} + H_{AE} + H_E, \quad (10)$$

containing terms describing the donors (D), the acceptors (A), the environment (E) and their interactions (mixed indices). Inspired by light-harvesting systems, which are weakly excited by sunlight, we assume only a single excitation in the system and model each donor and acceptor site as a two-level system. Donor sites D_j have energies E_j^D and interact through couplings $V_{jj'}^D$,

$$H_D = \sum_j E_j^D |D_j\rangle \langle D_j| + \sum_{j \neq j'} V_{jj'}^D |D_j\rangle \langle D_{j'}|. \quad (11)$$

Similarly, in the acceptor site basis,

$$H_A = \sum_k E_k^A |A_k\rangle \langle A_k| + \sum_{k \neq k'} V_{kk'}^A |A_k\rangle \langle A_{k'}|. \quad (12)$$

Donor and acceptor sites interact with each other through

$$H_{DA} = \sum_{j,k} V_{jk}^{DA} |D_j\rangle \langle A_k| + \text{h.c.} \quad (13)$$

The environment is modelled by coupling each site to an independent bath of harmonic oscillators,

$$H_E = \sum_j \sum_\xi \omega_{j\xi}^D a_{j\xi}^{D\dagger} a_{j\xi}^D + \sum_k \sum_\xi \omega_{k\xi}^A a_{k\xi}^{A\dagger} a_{k\xi}^A, \quad (14)$$

where $\hbar = 1$ and $a_{j\xi}^D$ is the annihilation operator for the ξ th environment mode of donor j . Similarly, $a_{k\xi}^A$ is the

operator for the ξ th mode on acceptor k . The system-environment interactions are assumed to be linear,

$$H_{DE} = \sum_j \sum_\xi g_{j\xi}^D (a_{j\xi}^D + a_{j\xi}^{D\dagger}) |D_j\rangle \langle D_j|, \quad (15)$$

$$H_{AE} = \sum_k \sum_\xi g_{k\xi}^A (a_{k\xi}^A + a_{k\xi}^{A\dagger}) |A_k\rangle \langle A_k|. \quad (16)$$

The system-environment interactions can be specified by their spectral densities, $J_j^D(\omega)$ for donors and $J_k^A(\omega)$ for acceptors, where

$$J_j^D(\omega) = \sum_\xi (g_{j\xi}^D)^2 \delta(\omega - \omega_\xi) \quad (17)$$

and similarly for $J_k^A(\omega)$. The strength of system-environment coupling is quantified by the reorganisation energy λ , defined for the j th donor as

$$\lambda_j^D = \int_0^\infty \frac{J_j^D(\omega)}{\omega} d\omega, \quad (18)$$

and similarly for acceptors. For simplicity, we assume the reorganisation energies of the donors are the same ($\lambda_j^D = \lambda^D$) and similarly for the acceptors ($\lambda_k^A = \lambda^A$).

The simplest model of supertransfer can be obtained using classical noise, which manifests itself as time-dependent fluctuations of site energies: $E_j^D \rightarrow E_j^D + \delta E_j^D(t)$, $E_k^A \rightarrow E_k^A + \delta E_k^A(t)$. Classical noise in site energies induces dephasing in the site basis, whose effect on transfer [20, 26] depends on its spectral density $J(\omega)$; here, we use, at each site, the Drude-Lorentz spectral density

$$J(\omega) = \frac{2\omega\lambda}{\omega^2 + \omega_c^2}, \quad (19)$$

where ω_c is a cutoff frequency. Additionally, we assume an ω_c large compared to system frequencies, which yields Markovian dephasing.

The initial eigenstate is the lowest-energy state of the donor aggregate, whose extent of delocalisation varies based on system parameters. By tuning these parameters, the donor aggregate can be prepared in either a fully localised or a fully delocalised state (fig. 1). To enact normal transfer, excitation is localised on a donor site, or, more generally, in a statistical mixture of donor sites in the density matrix $\sum_{j=1} p_j |D_j\rangle \langle D_j|$. By contrast, to enact supertransfer, the excitation starts in a delocalised state $|D_\alpha\rangle$.

We determine γ by numerical simulation of the dynamics, generated by H , of the system's reduced density matrix $\rho(t)$ (fig. 2). In the limit of weak donor-acceptor coupling, the dynamics is described by the rate equation in eq. (1) and γ is given by the golden-rule expression in eq. (2). To extract γ from the dynamics, we fit the acceptor population $P_A(t)$ to

$$P_A(t) = P_A^\infty (1 - e^{-\gamma t}), \quad (20)$$

where $P_A(t) = \sum_j \langle A_j | \rho(t) | A_j \rangle$ and P_A^∞ is the final acceptor population.

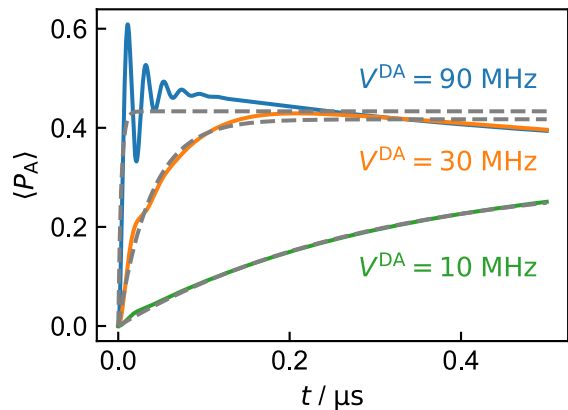


Figure 2. **Evaluating the transfer rate γ from population dynamics.** Population transfer to acceptor plotted for three values of donor-acceptor coupling V^{DA} with $\lambda^A = 80$ MHz and $\lambda^D = 10$ MHz. The solid lines are the numerically exact calculations of the acceptor populations, which are fitted to eq. (20) (dashed lines) to find the values of γ . The transfer is described by a rate equation when Rule 1 ($V^{\text{DA}} \ll \lambda^D + \lambda^A$) is met, as it is for $V^{\text{DA}} = 10$ MHz. At $V^{\text{DA}} = 30$ MHz, the exponential behaviour begins to break down, and it is a completely inaccurate description of the dynamics at $V^{\text{DA}} = 90$ MHz. Other parameter values are given in table 1. Calculations performed using QuTip [27].

III. DESIGN RULES FOR SUPERTRANSFER

There are two design rules for supertransfer, both of which take the form of time-scale separations.

Rule 1: the transfer must be well described by the golden-rule rate process of eq. (2). This requirement is met if the donor aggregate is weakly coupled to the acceptor aggregate, compared to the system-environment coupling quantified by the reorganisation energies,

$$|V^{\text{DA}}| \ll \lambda^D + \lambda^A. \quad (21)$$

Rule 2: the eigenstates of either the donor or the acceptor aggregates (or both) must be delocalised. For the donors (with the same applying for the acceptors), this can be achieved if the intra-aggregate couplings V^D are greater than both the static disorder in the aggregate (the variance δ^D of the set $\{E_j^D\}$) and the dynamic disorder (quantified by λ^D), i.e.,

$$V^D \gtrsim \delta^D, \lambda^D. \quad (22)$$

IV. EXPERIMENTAL PROPOSAL

The design rules above can be used to demonstrate supertransfer using a superconducting architecture.

The simplest case of supertransfer—shown in fig. 1—could be implemented by meeting three requirements. First, it requires three sites: two donors and one acceptor ($N_D = 2$ and $N_A = 1$). Second, the energies of these sites must be tunable to ensure that the acceptor energy is lower than those of the donors and to allow noise injection. Third, it must be possible to control delocalisation to show a higher transfer rate in the delocalised case compared to the localised one.

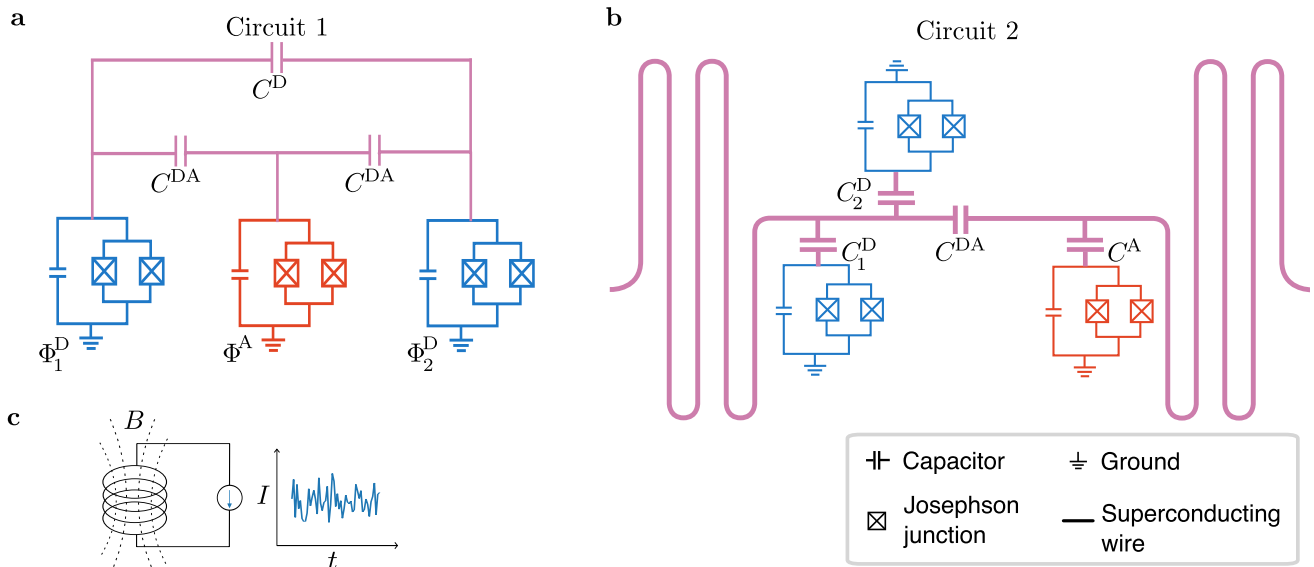


Figure 3. **Proposed superconducting circuit quantum electrodynamics (cQED) devices demonstrating controllable supertransfer.** Both circuits realise the model of fig. 1 using flux-tunable transmon qubits. **a)** In Circuit 1, the donors (blue) are coupled to each other directly through capacitors. **b)** In Circuit 2, the coupling between sites is mediated by two buses (purple). **c)** In both circuits, noise can be introduced using an independent solenoid on each site; fluctuating the current I through the solenoids produces fluctuating magnetic fluxes Φ through the transmon loops, changing their site energies.

Parameter	Value (MHz)	Implementation in Circuit 1	Implementation in Circuit 2
V^D	10	C^D	\tilde{C}^D
V^{DA}	10	C^{DA}	\tilde{C}^{DA}
$E^D - E^A$	148	$E^D - E^A$	$\tilde{E}^D - \tilde{E}^A$
δ^D	5	$\langle \delta E^D(t) \rangle$	$\langle \delta \tilde{E}^D(t) \rangle$
λ^D	10	λ_D^{cl}	$\tilde{\lambda}_D^{cl}$
λ^A	80	λ_A^{cl}	$\tilde{\lambda}_A^{cl}$

Table 1. **Sample of proposed parameters** for showing supertransfer in Circuit 1 and Circuit 2, being values that are experimentally feasible in cQED experiments [21].

These requirements are all achievable experimentally using a superconducting circuit quantum electrodynamics (cQED) architecture. In cQED, the sites can be implemented as transmon qubits whose energy can be tuned using an external magnetic field [28]. The couplings between the sites can be mediated either by capacitive couplings as in fig. 3a or using a bus as in fig. 3b.

The Hamiltonian of the required cQED circuit is

$$H_{\text{circuit}} = E^D \sigma_1^z + (E^D + \delta^D) \sigma_2^z + E^A \sigma_A^z + C^D \sigma_1^x \sigma_2^x + C^{DA} (\sigma_1^x \sigma_A^x + \sigma_2^x \sigma_A^x) + \text{h.c.}, \quad (23)$$

where σ_i^z and σ_i^x are Pauli operators for site i , while C^D and C^{DA} are couplings. For example, for donor 1, $\sigma_1^z = |D_1\rangle \langle D_1| - |G\rangle \langle G|$ and $\sigma_1^x = |D_1\rangle \langle G| + |G\rangle \langle D_1|$, where $|G\rangle$ is the state of the system with no excitations. H_{circuit} preserves the number of excitations and reduces to H when restricted to its single-excitation subspace.

Site energies are tunable because transmon energies are sensitive to external magnetic fields [21, 29, 30],

$$H_{\text{qb}} = E_{\text{qb}}(\Phi) \sigma_z. \quad (24)$$

The energy E_{qb} can be tuned between hardware-dependent values of E_{min} and E_{max} by tuning the mag-

netic flux Φ through the transmon's superconducting loop (fig. 3) from 0 to $\Phi_0\pi/2$, where $\Phi_0 = h/2e$ is the flux quantum [30]. Experimentally, $E_{\text{qb}}(\Phi)$ is typically tunable across a range $E_{\text{max}} - E_{\text{min}}$ of around 100 MHz, or, in some hardware, up to 1 GHz [29, 31, 32].

The tunability of flux-tunable transmons is used to engineer static disorders and also a dephasing environment by fluctuating the energy levels [20]. To generate the fluctuating flux $\Phi(t)$, a fluctuating current $I(t)$ is injected into a solenoid to generate a fluctuating magnetic field $B(t)$ as in fig. 3c. For small currents, the change in the energy of site i ($\delta E_i(t) = E_i(t) - \langle E_i(t) \rangle$) due to a change in current $\delta I(t)$ is

$$\delta E_i(t) \approx \frac{dE_i}{d\Phi_i} \frac{d\Phi_i}{dB_i} \frac{dB_i}{dI_i} \delta I_i(t), \quad (25)$$

where the product of the derivatives is a calibration factor that can be experimentally determined.

The mean of the fluctuations $\langle \delta E_i(t) \rangle$ gives the static disorder δ_i . The effect of the dynamic disorder induced by the classical noise signal $\delta E_i(t)$ is determined by its spectrum $J^{\text{cl}}(\omega)$, which is the Fourier transform of the

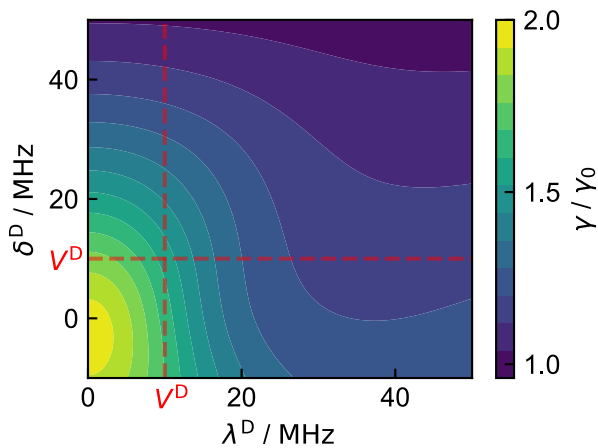


Figure 4. Donor parameters in Circuit 1 can be tuned to switch the dynamics from normal transfer at rate γ_0 to supertransfer at rate $2\gamma_0$. Supertransfer is achieved when Rule 2 is met, i.e., the reorganisation energy λ^D and the site detuning δ_{DD} are both smaller than the intra-aggregate coupling V^D , as is the case in the bottom-left of the plot. The rate gradually transitions to that of normal transfer as either parameter moves away from this region. The other parameter value are as in table 1, giving $\gamma_0 = 0.77 \mu\text{s}^{-1}$.

site-energy correlation function,

$$J^{\text{cl}}(\omega) = \mathcal{F}\{\langle \delta E_i(t) \delta E_i(0) \rangle\}. \quad (26)$$

The overall effect of the noise is quantified by the reorganisation energy

$$\lambda^{\text{cl}} = \int_0^\infty \frac{J^{\text{cl}}(\omega)}{\omega} d\omega. \quad (27)$$

The final component, the controllable couplings between sites, can be realised in two different ways, as shown in fig. 3.

In *Circuit 1* (fig. 3a), the couplings C are implemented as direct capacitive couplings. These can be either fixed [33–35] or adjustable using a longitudinal electric field [36]. Capacitive coupling allows a direct implementation of the desired cQED Hamiltonian of eq. (23).

By contrast, in *Circuit 2* (fig. 3b), the couplings are mediated by buses [37–39]. This approach has the advantage of being more easily scalable to greater numbers of donors and acceptors. Bus-mediated coupling can be understood using the Hamiltonian of Circuit 2, where both of the donors are coupled to the donor bus (a microwave cavity resonator), the acceptor is coupled to the acceptor bus, and the two buses are capacitively coupled to each other,

$$H_2 = \sum_{i=1}^2 \left(E_i^D \sigma_i^z + C_i^D (b_D^\dagger \sigma_i^- + b_D \sigma_i^+) \right) + \omega_D b_D^\dagger b_D \\ + E^A \sigma_A^z + C^A (b_A^\dagger \sigma_A^- + b_A \sigma_A^+) + \omega_A b_A^\dagger b_A \\ + C^{\text{DA}} (b_D^\dagger + b_D)(b_A^\dagger + b_A), \quad (28)$$

where $\sigma^\pm = \sigma^x \pm i\sigma^y$, b_D and b_A are the donor and acceptor bus annihilation operators, ω_D and ω_A are the bus resonant frequencies, and C_i^D and C^A are the couplings of the qubits to their bus and C^{DA} couples

the two buses. When the sites are far detuned from ω_D and ω_A , the baths can be adiabatically eliminated using the Fröhlich-Nakajima transformation [39, 40] to give the effective Hamiltonian

$$H_{\text{eff}} = \sum_{i=1}^2 \tilde{E}_i^D |D_i\rangle \langle D_i| + \tilde{E}^A |A\rangle \langle A| + \tilde{C}^{\text{DD}} \sigma_1^- \sigma_2^+ \\ + \tilde{C}^{1A} \sigma_1^- \sigma_A^+ + \tilde{C}^{2A} \sigma_2^- \sigma_A^+ + \text{h.c.}, \quad (29)$$

where the effective couplings and energies are

$$\tilde{C}^{\text{DD}} = \frac{C_1^D}{2\Delta_1} \frac{C_2^D}{2\Delta_2} (\Delta_1 + \Delta_2), \quad (30)$$

$$\tilde{C}^{iA} = C^{\text{DA}} \frac{C_i^D}{\Delta_i} \frac{C^A}{\Delta_A}, \quad (31)$$

$$\tilde{E}_i^D = 2E_i^D + \frac{(C_i^D)^2}{\Delta_i}, \quad (32)$$

$$\tilde{E}^A = 2E^A + \frac{(C^A)^2}{\Delta_A}, \quad (33)$$

with $\Delta_i = 2E_i^D - \omega_D$ and $\Delta_A = 2E^A - \omega_A$.

The noise spectrum $\tilde{J}^{\text{cl}}(\omega)$ due to fluctuations of E_i^D and E^A is given by the Fourier transform of $\langle \delta \tilde{E}(t) \delta \tilde{E}(0) \rangle$, and the reorganisation energy $\tilde{\lambda}^{\text{cl}}$ by eq. (27).

Simulation results. We simulate the dynamics in Circuit 1 with the parameters in table 1 using QuTip [27]. These parameters are chosen because they meet Rule 1 and Rule 2 for supertransfer and are representative of typical values found in cQED systems [21].

When Rule 1 ($V^{\text{DA}} \ll \lambda^D + \lambda^A$) is met, the transfer is exponential (fig. 2). The exponential behaviour breaks down and becomes oscillatory for $V^{\text{DA}} \gtrsim \lambda$.

When Rule 2 ($V^D \gtrsim \delta^D, \lambda^D$) is met, the supertransfer enhances the transfer rate γ (fig. 4). The maximum supertransfer rate $2\gamma_0$ (for $N_D = 2$ and $N_A = 1$) gradually decreases to γ_0 if the donor parameters leave the region defined by Rule 2. This gradual change with the parameters makes supertransfer robust to small changes in either the static (δ) or dynamic (λ) disorders.

Scaling of supertransfer with the number of donors and acceptors. The supertransfer rate increases in proportion to the number of sites participating in the delocalised donor and acceptor aggregates, according to eq. (9). This scaling could be experimentally demonstrated by adding more donor and acceptor sites to Circuit 2, as shown in fig. 5a. In this enlarged circuit, the number of participating qubits can be adjusted by detuning undesired qubits out of the dynamics. The simulation results in fig. 5b confirm the scaling law of eq. (9).

V. DISCUSSION

We showed that a quantum device based on a cQED circuit could be engineered to conclusively demonstrate supertransfer. The simplest supertransfer case is achieved with $N_D = 2$ and $N_A = 1$, with larger arrangements also possible, as shown in fig. 5.

Circuits 1 and 2 are achievable with current engineering capabilities in cQED, as all required components have been experimentally demonstrated. The necessary couplings can be implemented using either of

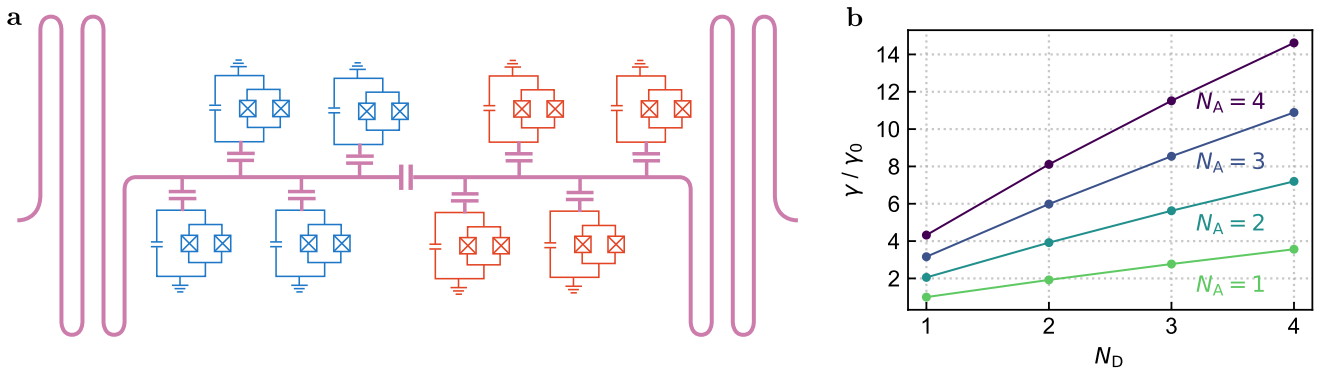


Figure 5. **Supertransfer scaling with the number of donors and acceptors.** **a)** Expansion of Circuit 2 for demonstrating the scaling of the transfer rate. The donors are connected through a bus and the acceptors are connected through a second bus capacitively coupled to the first. The number of donors or acceptors participating in the dynamics could be changed on the fly by detuning the energy of unwanted qubits to be much higher than the others. **b)** Transfer rates, obtained by fitting simulated acceptor populations using eq. (20). The rate increases as $O(N_D N_A)$, as expected in supertransfer. For large N_A and N_D , the rate is slightly smaller than the predicted $N_D N_A \gamma_0$ because eigenstate energies change slightly as additional sites are added. The other parameter value are as in table 1, giving $\gamma_0 = 0.77 \mu\text{s}^{-1}$.

two established experimental techniques: direct capacitive coupling [33–35] or buses for indirect qubit coupling [29, 38, 41]. Furthermore, the ability to inject noise into the system has also been demonstrated for both the Drude-Lorentz spectrum we use and for more general ones [20, 42, 43]. Finally, our proposal can be implemented using simulation times that are an order of magnitude shorter than typical transmon decoherence times of 50–120 μs [21].

The two proposed implementations—direct coupling in Circuit 1 and indirect coupling in Circuit 2—have complementary advantages. In Circuit 1, there is complete flexibility in selecting all of the couplings, which means that the mapping of the supertransfer Hamiltonian is direct and straightforward. However, the implementation of all-to-all connectivity would be challenging when Circuit 1 is scaled up to more donors and acceptors. In contrast, in Circuit 2, the couplings are achieved through a bus, facilitating scalability as illustrated in fig. 5a. However, the scalability comes at the cost of a less straightforward mapping of the supertransfer Hamiltonian and limited flexibility in tuning the parameters, because tuning one circuit parameter can

affect multiple parameters in the effective Hamiltonian (see eq. (29)). Circuit 2 has the further advantage that its detuning-based couplings allow for negative couplings, which opens possibilities such as rearranging the order of bright $|+\rangle$ and dark $|-\rangle$ states.

The robustness of supertransfer to experimental noise simplifies implementation by reducing the need for precise parameter engineering. It is feasible in any system provided that conditions specified by Rule 1 and Rule 2 are satisfied. Furthermore, the resilience to variations in system parameters and environmental conditions may enable applications of supertransfer in quantum-enhanced engineered systems.

ACKNOWLEDGEMENTS

We thank Francesco Campaioli, Jared Cole, Xanthe Croot, and Alexander Grimm for valuable discussions. We were supported by the Australian Research Council (DP220103584 and FT230100653) and a Sydney Quantum Academy scholarship.

* ivan.kassal@sydney.edu.au

- [1] R. H. Dicke, Coherence in spontaneous radiation processes, *Phys. Rev.* **93**, 99 (1954).
- [2] M. Gross and S. Haroche, Superradiance: An essay on the theory of collective spontaneous emission, *Phys. Rep.* **93**, 301–396 (1982).
- [3] K. D. B. Higgins, S. C. Benjamin, T. M. Stace, G. J. Milburn, B. W. Lovett, and E. M. Gauger, Superabsorption of light via quantum engineering, *Nat. Commun.* **5**, 4705 (2014).
- [4] J. Q. Quach, K. E. McGhee, L. Ganzer, D. M. Rouse, B. W. Lovett, E. M. Gauger, J. Keeling, G. Cerullo, D. G. Lidzey, and T. Virgili, Superabsorption in an organic microcavity: Toward a quantum battery, *Sci. Adv.* **8**, eabk3160 (2022).
- [5] J. Q. Quach and W. J. Munro, Using Dark States to Charge and Stabilize Open Quantum Batteries, *Phys. Rev. Appl.* **14**, 024092 (2020).
- [6] J. Quach, G. Cerullo, and T. Virgili, Quantum batteries: The future of energy storage?, *Joule* **7**, 2195–2200 (2023).
- [7] W. Stręk, Cooperative energy transfer, *Phys. Lett. A* **62**, 315 (1977).
- [8] H. Sumi, Theory on Rates of Excitation-Energy Transfer between Molecular Aggregates through Distributed Transition Dipoles with Application to the Antenna System in Bacterial Photosynthesis, *J. Phys. Chem. B* **103**, 252–260 (1998).
- [9] S. Lloyd and M. Mohseni, Symmetry-enhanced supertransfer of delocalized quantum states, *New J. Phys.* **12**, 075020 (2010).
- [10] M. Merkli, G. P. Berman, and R. Sayre, Electron transfer reactions: generalized spin-boson approach, *J. Math. Chem.* **51**, 890 (2012).

- [11] S. Baghbanzadeh and I. Kassal, Geometry, supertransfer, and optimality in the light harvesting of purple bacteria, *J. Phys. Chem. Lett.* **7**, 3804–3811 (2016).
- [12] N. B. Taylor and I. Kassal, Generalised marcus theory for multi-molecular delocalised charge transfer, *Chem. Sci.* **9**, 2942 (2018).
- [13] K. Mukai, S. Abe, and H. Sumi, Theory of Rapid Excitation-Energy Transfer from B800 to Optically-Forbidden Exciton States of B850 in the Antenna System LH2 of Photosynthetic Purple Bacteria, *J. Phys. Chem. B* **103**, 6096–6102 (1999).
- [14] S. Tomasi and I. Kassal, Classification of Coherent Enhancements of Light-Harvesting Processes, *J. Phys. Chem. Lett.* **11**, 2348 (2020).
- [15] G. D. Scholes and G. R. Fleming, On the Mechanism of Light Harvesting in Photosynthetic Purple Bacteria: B800 to B850 Energy Transfer, *J. Phys. Chem. B* **104**, 1854–1868 (2000).
- [16] G. D. Scholes, Long-Range Resonance Energy Transfer in Molecular Systems, *Annu. Rev. Phys. Chem.* **54**, 57–87 (2003).
- [17] S. Baghbanzadeh and I. Kassal, Distinguishing the roles of energy funnelling and delocalization in photosynthetic light harvesting, *Phys. Chem. Chem. Phys.* **18**, 7459–7467 (2016).
- [18] S. Tomasi, D. M. Rouse, E. M. Gauger, B. W. Lovett, and I. Kassal, Environmentally Improved Coherent Light Harvesting, *J. Phys. Chem. Lett.* **12**, 6143 (2021).
- [19] D. M. Rouse, A. Kushwaha, S. Tomasi, B. W. Lovett, E. M. Gauger, and I. Kassal, Light-Harvesting Efficiency Cannot Depend on Optical Coherence in the Absence of Orientational Order, *J. Phys. Chem. Lett.* **15**, 254–261 (2024).
- [20] A. Potočník, A. Bargerbos, F. A. Y. N. Schröder, S. A. Khan, M. C. Collodo, S. Gasparinetti, Y. Salathé, C. Creatore, C. Eichler, H. E. Türeci, A. W. Chin, and A. Wallraff, Studying light-harvesting models with superconducting circuits, *Nat. Commun.* **9**, 904 (2018).
- [21] A. Blais, A. L. Grimsmo, S. Girvin, and A. Wallraff, Circuit quantum electrodynamics, *Rev. Mod. Phys.* **93**, 025005 (2021).
- [22] C. W. Kim, J. M. Nichol, A. N. Jordan, and I. Franco, Analog quantum simulation of the dynamics of open quantum systems with quantum dots and microelectronic circuits, *PRX Quantum* **3**, 040308 (2022).
- [23] V. May and O. Kühn, *Charge and Energy Transfer Dynamics in Molecular Systems* (Wiley, 2011).
- [24] S. Tomasi and I. Kassal, Classification of coherent enhancements of light-harvesting processes, *J. Phys. Chem. Lett.* **11**, 2348 (2020).
- [25] K. D. B. Higgins, B. W. Lovett, and E. M. Gauger, Quantum-Enhanced Capture of Photons Using Optical Ratchet States, *J. Phys. Chem. C* **121**, 20714–20719 (2017).
- [26] Q. Huang and M. Merkli, Qubit dynamics with classical noise, *Phys. Open* **5**, 100043 (2020).
- [27] J. Johansson, P. Nation, and F. Nori, QuTiP 2: A Python framework for the dynamics of open quantum systems, *Comput. Phys. Commun.* **184**, 1234–1240 (2013).
- [28] J. Koch, T. M. Yu, J. Gambetta, A. A. Houck, D. I. Schuster, J. Majer, A. Blais, M. H. Devoret, S. M. Girvin, and R. J. Schoelkopf, Charge-insensitive qubit design derived from the Cooper pair box, *Phys. Rev. A* **76**, 042319 (2007).
- [29] L. DiCarlo, J. M. Chow, J. M. Gambetta, L. S. Bishop, B. R. Johnson, D. I. Schuster, J. Majer, A. Blais, L. Frunzio, S. M. Girvin, and R. J. Schoelkopf, Demonstration of two-qubit algorithms with a superconducting quantum processor, *Nature* **460**, 240–244 (2009).
- [30] P. Krantz, M. Kjaergaard, F. Yan, T. P. Orlando, S. Gustavsson, and W. D. Oliver, A quantum engineer’s guide to superconducting qubits, *Appl. Phys. Rev.* **6**, 021318 (2019).
- [31] J. A. Schreier, A. A. Houck, J. Koch, D. I. Schuster, B. R. Johnson, J. M. Chow, J. M. Gambetta, J. Majer, L. Frunzio, M. H. Devoret, S. M. Girvin, and R. J. Schoelkopf, Suppressing charge noise decoherence in superconducting charge qubits, *Phys. Rev. B* **77**, 180502 (2008).
- [32] M. A. Rol, L. Ciorciaro, F. K. Malinowski, B. M. Tarasinski, R. E. Sagastizabal, C. C. Bultink, Y. Salathe, N. Haandbaek, J. Sedivy, and L. DiCarlo, Time-domain characterization and correction of on-chip distortion of control pulses in a quantum processor, *Appl. Phys. Lett.* **116**, 054001 (2020).
- [33] Y. A. Pashkin, T. Yamamoto, O. Astafiev, Y. Nakamura, D. V. Averin, and J. S. Tsai, Quantum oscillations in two coupled charge qubits, *Nature* **421**, 823–826 (2003).
- [34] A. J. Berkley, H. Xu, R. C. Ramos, M. A. Gubrud, F. W. Strauch, P. R. Johnson, J. R. Anderson, A. J. Dragt, C. J. Lobb, and F. C. Wellstood, Entangled Macroscopic Quantum States in Two Superconducting Qubits, *Science* **300**, 1548–1550 (2003).
- [35] R. C. Bialczak, M. Ansmann, M. Hofheinz, E. Lucero, M. Neeley, A. D. O’Connell, D. Sank, H. Wang, J. Wenner, M. Steffen, A. N. Cleland, and J. M. Martinis, Quantum process tomography of a universal entangling gate implemented with Josephson phase qubits, *Nat. Phys.* **6**, 409–413 (2010).
- [36] Y. Wu, L.-P. Yang, M. Gong, Y. Zheng, H. Deng, Z. Yan, Y. Zhao, K. Huang, A. D. Castellano, W. J. Munro, K. Nemoto, D.-N. Zheng, C. P. Sun, Y. xi Liu, X. Zhu, and L. Lu, An efficient and compact switch for quantum circuits, *npj Quantum Inf.* **4**, 50 (2018).
- [37] A. Blais, R.-S. Huang, A. Wallraff, S. M. Girvin, and R. J. Schoelkopf, Cavity quantum electrodynamics for superconducting electrical circuits: An architecture for quantum computation, *Phys. Rev. A* **69**, 062320 (2004).
- [38] J. Majer, J. M. Chow, J. M. Gambetta, J. Koch, B. R. Johnson, J. A. Schreier, L. Frunzio, D. I. Schuster, A. A. Houck, A. Wallraff, A. Blais, M. H. Devoret, S. M. Girvin, and R. J. Schoelkopf, Coupling Superconducting Qubits via a Cavity Bus, *Nature* **449**, 443 (2007).
- [39] M. Tao, M. Hua, N. Zhang, W. He, Q. Ai, and F. Deng, Quantum simulation of clustered photosynthetic light harvesting in a superconducting quantum circuit, *Quantum Eng.* **2**, e53 (2020).
- [40] A. Blais, J. Gambetta, A. Wallraff, D. I. Schuster, S. M. Girvin, M. H. Devoret, and R. J. Schoelkopf, Quantum-information processing with circuit quantum electrodynamics, *Phys. Rev. A* **75**, 032329 (2007).
- [41] C. Song, K. Xu, W. Liu, C.-p. Yang, S.-B. Zheng, H. Deng, Q. Xie, K. Huang, Q. Guo, L. Zhang, P. Zhang, D. Xu, D. Zheng, X. Zhu, H. Wang, Y.-A. Chen, C.-Y. Lu, S. Han, and J.-W. Pan, 10-qubit Entanglement and Parallel Logic Operations with a Superconducting Circuit, *Phys. Rev. Lett.* **119**, 180511 (2017).
- [42] P. Solinas, M. Möttönen, J. Salmilehto, and J. P. Pekola, Cooper-pair current in the presence of flux noise, *Phys. Rev. B* **85**, 024527 (2012).
- [43] Y. Sung, A. Vepsäläinen, J. Braumüller, F. Yan, J. I.-J. Wang, M. Kjaergaard, R. Winik, P. Krantz, A. Bengtsson, A. J. Melville, B. M. Niedzielski, M. E. Schwartz, D. K. Kim, J. L. Yoder, T. P. Orlando, S. Gustavsson, and W. D. Oliver, Multi-level quantum noise spectroscopy, *Nat. Commun.* **12**, 967 (2021).